

Optimization of Coil Parameters for a Nonlinear Two Degree-of-Freedom (2DOF) Velocity-amplified Electromagnetic Vibrational Energy Harvester

Eliabetta Boco¹, Valeria Nico¹, Declan O'Donoghue¹, Ronan Frizzell², Gerard Kelly² and Jeff Punch¹

¹*CTVR, Stokes Institute, University of Limerick, Plassey, Limerick, Ireland*

²*Efficient Energy Transfer (η ET) Dept, Bell Labs, Alcatel-Lucent, Dublin, Ireland*

Keywords: Energy Harvesting, Nonlinearity, Multiple Degree of Freedom, Electromagnetic Optimization, Modelling.

Abstract: A 2DOF velocity amplified electromagnetic vibrational energy harvester is analyzed. The system consists of two masses, one larger than the other, oscillating relative to each other in response to external excitation. The large mass is designed with a centrally located cavity into which a second smaller mass is placed. This configuration allows the larger mass to impart momentum to the smaller mass during impact, which significantly amplifies the velocity of the smaller mass. By coupling high strength magnets (placed on the larger mass) and a coil (embedded in the smaller mass), an electric current is induced in the coil through the relative motion of the two masses. To intensify the magnetic field, the magnets are arranged with alternating polarity within the soft-iron body of the larger mass. Between the two masses, and between the larger mass and the support, four springs are placed. The smaller mass is designed to disconnect from the larger mass, when input vibrations of sufficient magnitude are present, and this leads to significant nonlinearity in the system response, which is well described by its transfer function. The nonlinearity leads to an increased bandwidth over which the system can harvest energy. As a further improvement, the energy harvester is optimized by changing the properties of the coil. Four different coils are compared in terms of their voltage and power output. Finally, a theoretical model is proposed in order to predict the optimal configuration.

1 INTRODUCTION

From the invention of the first transistor in 1947 made by John Bardeen, Walter Brattain, and William Shockley, the number of transistors in Integrated Circuits (ICs) has followed Moore's law, basically doubling approximately every two years. An increasing number of transistors, however, has not only led to more powerful devices, but also increased power consumption. Moreover, nowadays Information and Communication Technologies (ICTs) are used in almost all fields of everyday life, so that the global power demand is constantly increasing, mainly involving a greater number of sensors and micro and nano-scales device (i.e. wireless sensors networks for temperature or pressure in buildings, industrial plants or in the environment). Energy harvesting comes from the necessity to address this increasing power demand and aims to extract energy already present in the environment in many forms, such as temperature gradients, vibrations and electromagnetic waves, and use this energy to power low-power consuming elec-

tronic devices.

Vibrations are one of the most appealing kinds of ambient energy: they are always present, at any scale, and their intensity can be very different depending on the surrounding conditions. There are many possible ways to convert vibrational energy: piezoelectric, electromagnetic or variable capacitors. In this work, the electromagnetic conversion method is used, because it is applicable at many scales and it can produce quite high power densities provided that there is high relative velocity between the magnet and coil (Waters et al., 2008). Nonlinear systems are advantageous compared to linear systems since although linear systems have a higher response at resonance, nonlinear systems are more flexible because they do not need to be tuned, i.e. they are naturally able to harvest energy from broad band excitations. In this manner, a single nonlinear device can be used in many different applications and can be efficient even if the excitation frequency spectrum is not constant in time, which is a feature of many real vibration profiles (Cottone et al., 2009; Leadenham and Erturk, 2014).

The first part of the paper presents the experimental characterization of a two degree-of-freedom (2DOF) velocity-amplified electromagnetic energy harvester. To exploit nonlinearities, and to provide velocity amplification, an uncoupled 2DOF system is used: a 2DOF harvester can enlarge the energy conversion bandwidth (Wu et al., 2012b; Wu et al., 2012a; Jang et al., 2011), but it does not improve the harvesting capability for random excitations as long as the masses are coupled (Jang et al., 2012). Moreover, for electromagnetic conversion the most important feature is the high relative velocity between coil and magnets: in order to have velocity amplification through the momentum transfer between two impacting masses, the masses need to be uncoupled. A transfer function analysis is used to describe the observed nonlinearity in detail. Following this, an optimization process for designing the coil of the electromagnetic generator is proposed. Finally, a numerical model is presented, which can be used to predict the optimal coil settings for a given volume.

2 TRANSFER FUNCTION CHARACTERISATION

The main purpose of this section is to investigate the nonlinear response of a 2DOF vibration energy harvester. In order to do so, the system was tested experimentally under different levels of acceleration and the transfer function is used to highlight nonlinearities in the system response.

2.1 Experimental Setup and Procedure

The system consists of a large mass, where four magnets are orientated in the configurations shown in Fig.1. The large mass can move between two springs which are attached to the outer housing that serve to transfer energy from the vibrating base into the larger mass itself. A smaller mass, enclosed within the cavity of the larger mass is designed to separate from the larger mass when sufficient excitation is present. This configuration allows the larger mass to impart momentum to the smaller mass during impact, which significantly amplifies the velocity of the smaller mass. (Cottone et al., 2014; Nico et al., 2014; O'Donoghue et al., 2014). All impacting surfaces have high Q springs attached to mediate the impacts and efficiently transfer loads. The volume of the outside mass is $1.29 \cdot 10^{-4} \text{ m}^3$. The closed loop system used to control the LDS V406 permanent magnet shaker from Bruel&Kjaer is shown schematically in Fig.2. Output signals from the Dactron Comet shaker control

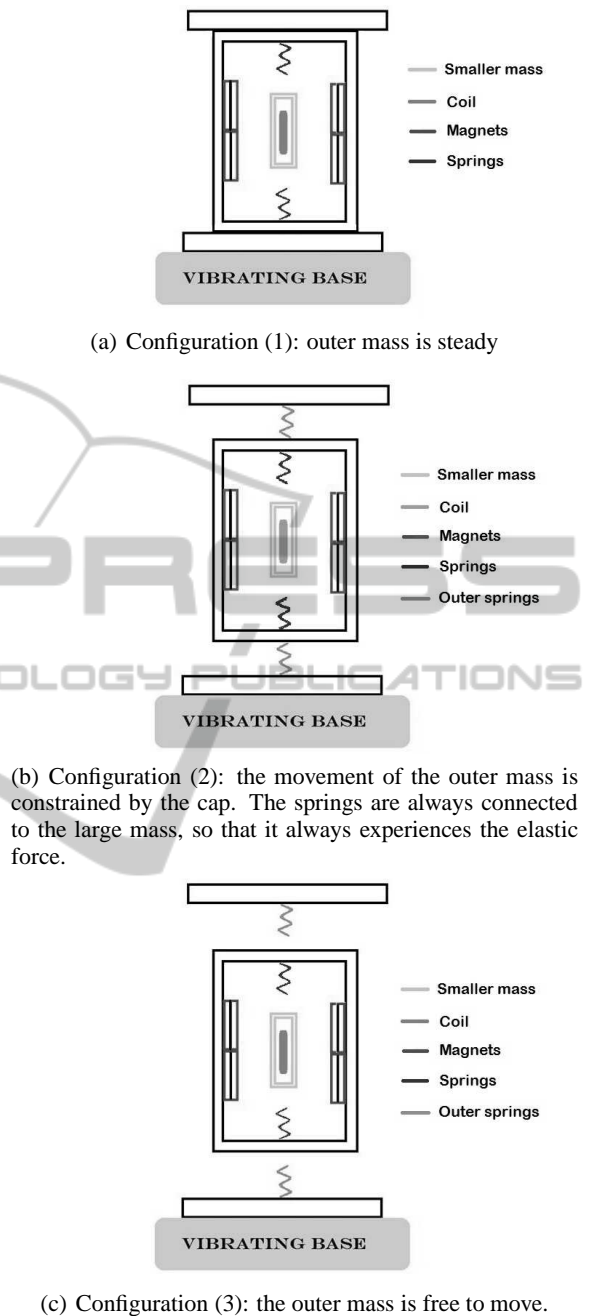


Figure 1: Schematic of the 2DOF energy harvester. The coil is embedded in a smaller mass which oscillates between four magnets that provide a strong magnetic field. The big mass oscillates outside in configuration (2) and (3) while it is fixed in configuration (1). The collisions between the two masses provide the velocity amplification.

system were amplified using the LDS TPO 25 Power Oscillator and used to drive the shaker and the voltage response of the harvester for each coil was measured using LabView through an appropriate data acquisition card. For each coil, data have been acquired using

the load resistance which maximized the power output. A high sensitivity ($1.96mV/g$) PCB Piezotronic accelerometer was employed to provide feedback to the controller in order to ensure that the correct acceleration levels were applied.

To fully characterize the system, two configurations were tested (see Fig.1 (a) and (b)): (1) motion of the larger mass was prevented and so only the smaller mass was free to oscillate and (2) motion of the smaller mass was free but motion of the larger mass was restricted by the top of the housing which was lowered to ensure the larger mass could not detach from its supporting springs (this meant that spring forces were always active on the larger mass). These configurations allowed different modes of operation of the 2DOF system to be investigated to better understand the response of the system.

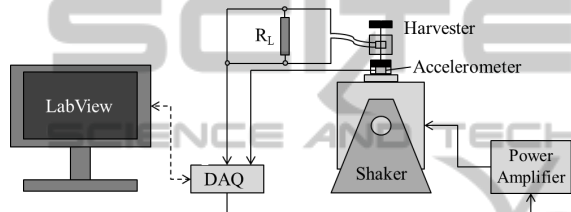


Figure 2: Experimental setup.

In configuration (1), the response of the smaller mass could be investigated in isolation, while the coupled response was examined using configuration (2). The response of each of these configurations varied considerably depending on the magnitude of the input acceleration, as this controlled whether the masses decouple from each other or not. For example, when the input acceleration was sufficiently low (from $a=0.05g$ to $a=0.2g$) the larger mass did not oscillate in any configuration and the spring on the underside of the smaller mass remained in contact with the larger mass. Under such excitation levels, configuration (1) behaved linearly, while system (2) could be considered to be a pair of coupled harmonic oscillators. In addition there were further nonlinearities due to the electromagnetic conversion.

Under higher levels of excitation ($a=0.5g$), the smaller mass in configuration (1) received sufficient energy to break contact with the larger mass, leading to nonlinearity in the system response. This was caused by the fact that while the smaller mass is detached from larger mass, there is no elastic spring force acting on it. This means that the effective elastic constant experienced by the system depends on the time that each mass is moving freely in the detached configuration. Higher accelerations also allowed such changes in the system's effective elastic constants to affect configuration (2), resulting in the system acting

as coupled 2DOF oscillators with a softening nonlinearity.

To verify these empirical observations, the different configurations were tested under increasing and decreasing sine wave frequency sweeps (from 5 to 100 Hz in 260 seconds) with different amplitudes of accelerations, as in Fig.3 and Fig.4, and the voltage output was recorded. Finally, the transfer function was calculated for each configuration as described in the following section.

2.2 Transfer Function Analysis

Let $y(t)$ be the output of our system, and let $x(t)$ be the input. Let $X(f)$ and $Y(f)$ be the Laplace transforms of the input and the output respectively.

$$X(s) = \int_{-\infty}^{+\infty} x(t)e^{-st} dt \quad (1)$$

$$Y(s) = \int_{-\infty}^{+\infty} y(t)e^{-st} dt \quad (2)$$

Where

$$s = j\omega \quad (3)$$

The Laplace transform is equal to the Fourier transform, and represents the frequency behaviour of the system.

So, for a linear system, the transfer function is defined as:

$$H(\omega) = \frac{Y(\omega)}{X(\omega)} \quad (4)$$

When the system is linear, $H(\omega)$ is a well-defined mathematical function, because it has a unique value for each value of ω , whereas for a nonlinear system it depends also on the shape and amplitude of the input signal. This means that the transfer function is not mathematically well defined for nonlinear systems.

Nonetheless, transfer function analysis is a very useful method to know if a system is linear or not for different input signals, (Muller and Massarani, 2001), as deviations from linearity result in distinct variations in the transfer function, as will be discussed in the next section.

2.3 Transfer Function Results

Comparing the resulting spectrum from the transfer function analysis in Fig.3 to a simple linear response is the first method to detect nonlinearity in a system.

A linear response is characterized by a sharp resonant peak that is symmetric about that peak. Fig.3 shows that nonlinearity due to the change in the effective stiffness of the springs is evident as the acceleration increases. This is caused by the smaller

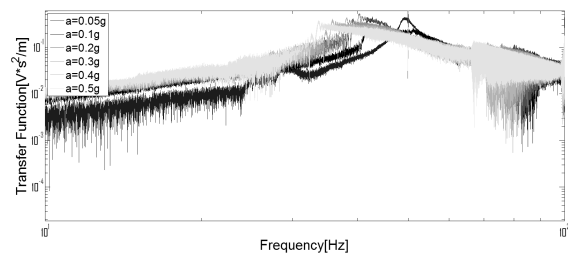
mass spending more and more time detached from the springs with increasing acceleration which led to a reduction of the resonant frequency of the system due to a decrease in the effective stiffness, an effect that is more pronounced for higher acceleration levels. The overall shape of the power spectrum varies for the different cases indicating deviation from linear behaviour. For example at very low acceleration amplitude ($a=0.05g$), in configuration (1), the behaviour is linear and the resonant peak is sharp and symmetric, as shown in Fig.3 (b). By increasing the acceleration, the resonant frequency decreases to lower frequencies becoming more and more asymmetric but displaying a broader band response (Fig.3 (a)). Very similar responses are seen for configuration (2) in Fig.4 (a) and (b)

The second fingerprint of nonlinearity in the transfer function characterization is the hysteresis phenomenon. In a linear system, a sine sweep that is increasing or decreasing in frequency as the excitation signal results in the same system response. In a nonlinear system, however, the behaviour for increasing or decreasing sweeps are different: as already stated, the transfer function is not a mathematically well-defined function for nonlinear systems as it can have two possible values for the same input frequency, one for the increasing sweep and one for the decreasing sweep (Leadenham and Erturk, 2014). The transfer function analysis in Fig.3 shows this hysteresis for configuration (1).

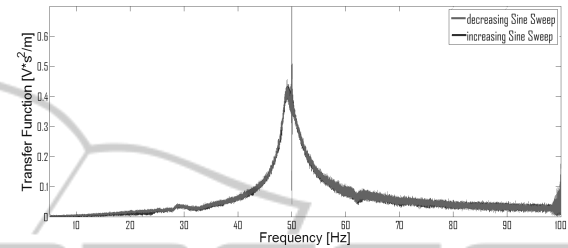
The same analysis has also been conducted using configuration (2), in order to investigate the effect of the impacts (Fig.4). The frequency shifting is quite similar when the outer mass started to fully compress the springs Fig.4 (c), (d) and (e). Then the effect of the velocity amplification became dominant, and the frequency response shifted to very low frequency, due to the larger mass, and the output increased by about an order of magnitude Fig.4 (b). The noisy behaviour outside resonance is due to the fact that using the sine sweep method to measure the transfer function is not the most robust to noise (Muller and Massarani, 2001).

An alternative more precise method, is an analysis through single harmonics excitation. This method is slower than a sine sweep, however, and since the non-linear effects are very well evident despite the noise, it was not considered necessary.

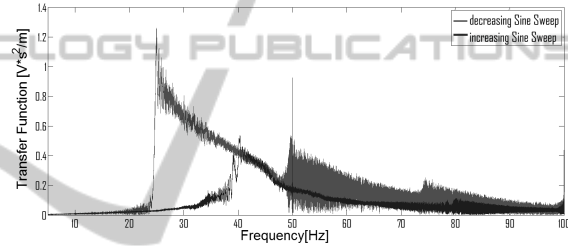
Improvements to the results could be achieved by conducting a statistically relevant number of tests and averaging them. The main problem with linear oscillators as energy harvesters, is that they are only able to harvest energy effectively from a narrow frequency range around their natural resonance. This



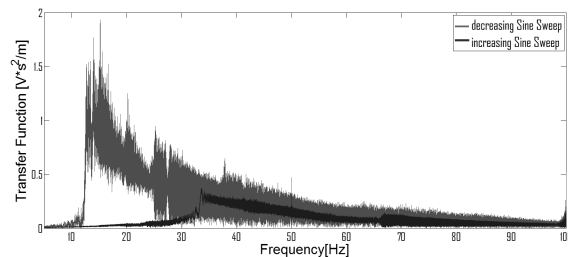
(a) Transfer function with the outer mass steady



(b) Hysteresis in the almost linear case. The output has been acquired at $a=0.05g$ so that the smaller mass cannot detach from the springs



(c) Hysteresis with $a=0.2g$ acceleration. The acceleration in input is $a=0.2g$, so that the smaller mass is starting to detach from the springs



(d) Hysteresis with $a=0.5g$ acceleration. The acceleration $a=0.5g$ is enough to let the smaller mass detach from the springs and spend more time decoupled from the larger mass leading to a decrease in the resonant frequency.

Figure 3: Measured transfer functions and hysteresis for configuration (1).

leads to a serious difficulty when reducing linear oscillator in size as, the smaller the system the higher the resonance frequency: a mm scale harvester would have a natural frequency in the kHz range, whereas real-world vibrations are usually under few thousands of Hz (Mizuno and Chetwynd, 2003; Rebeiz et al., 1987).

High natural frequencies are not compatible with

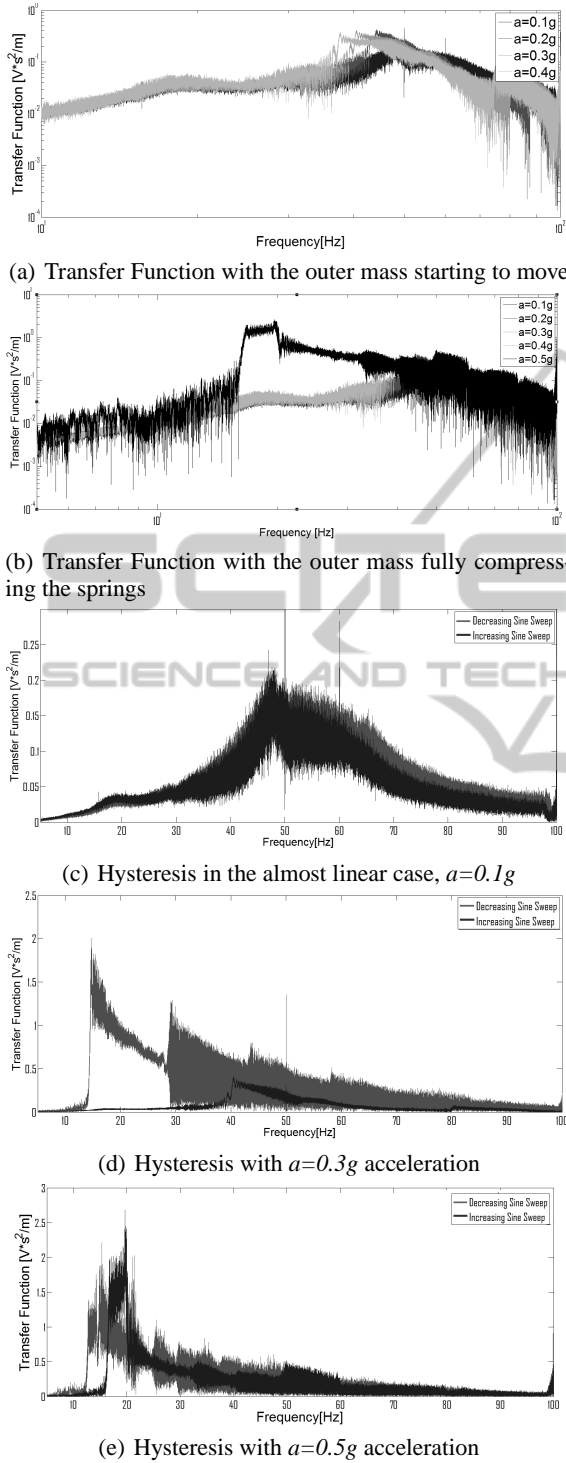


Figure 4: Measured Transfer Functions and Hysteresis for configuration (2).

many real-world vibrations, which are often characterised by low frequency, broad spectrum and are usually not constant in time. The analysis conducted here reveals that the response of a nonlinear energy har-

vester is more suitable for a broad band excitation, and that the scale is not the only factor to determine the frequency response, since the softening effect can also shift the resonance. There is the possibility also to use the nonlinear response to control the resonance frequency, however how much control is possible will need to be determined on a system-by-system basis.

3 OPTIMIZATION

3.1 Theoretical Model

An electromagnetic energy harvester can be described by a system of two coupled equations: the first is the equation of motion of the device, the second is the voltage output. The value of the magnetic flux into the coil acts as the coupling coefficient. (Bouendeu et al., 2011; Poulin et al., 2004). In this paper, a numerical model is proposed to predict the optimum coil parameters for a given magnetic field. Of particular interest are the wire diameter and number of turns that optimize the voltage and power output of the harvester.

The procedure used in this analysis was to select different wire diameters for a fixed internal radius and coil height, and then determine the resulting coil parameters; namely the coil length (l), coil resistance (R_C) and coil inductance (L). The parameters for the different wire diameters were then used to solve the system equations for a single-dof (1DOF) system as in configuration (1) in order to determine the optimum wire diameter.

The system to solve is:

$$\begin{cases} M\ddot{z} = -k_{eff}z - \gamma\dot{z} - \frac{BIV}{R_L} - A \sin(\omega t) \\ \dot{V} = \frac{R_L}{L}(Bl\dot{z} - \frac{R_C}{R_L}V - V) \end{cases} \quad (5)$$

where z is the relative displacement between the magnet and coil, M is the inertial mass, γ is the mechanical damping, B is the magnetic field, l is the length of the wire, R_L is the load resistance, L is the inductance, R_C is the coil resistance and V is the induced voltage.

To be able to predict the optimum coil wire diameter, the coil internal radius (r_i), the number of turns (N_{turns}) and the wire diameter itself (d_w) have been fixed in each simulation. From these parameters, it is possible to obtain:

$$N_{turns}_h = \frac{tf}{d} \quad (6)$$

where N_{turns}_h is number of wire turns along the height of the coil, t is the thickness of the coil, f is the fill factor and d is the diameter of the wire.

$$N_{turns_{surf}} = \frac{N_{turns} f}{N_{turns_h}} \quad (7)$$

where $N_{turns_{surf}}$ is the number of wire turns along the radial direction.

The outer radius of the coil is dependent on the number of turns and on the wire radius:

$$r_o = r_i + d N_{turns_{surf}} \quad (8)$$

where r_o and r_i are respectively the outer and the inner radius of the coil.

The coil length is given by:

$$l = N_{turns}(r_o + r_i)\pi; \quad (9)$$

The coil resistance can be determined from the wire length and resistivity:

$$R_c = \frac{\rho l}{(\pi(D/2)^2)} \quad (10)$$

where R_c is the coil resistance, ρ is the resistivity of the wire and D is the diameter of the coil.

The coil inductance (given in μH) can then be determined from Wheelers formula (Wheeler, 1942; Wheeler, 1928):

$$L = 0.02 \frac{[(r_o + r_i)/2]^2 N_{turns}^2}{6(r_o + r_i)/2 + 9t + 10(r_o - r_i)} \quad (11)$$

where r_o , r_i , t are in mm.

The mass of the coil is given by:

$$m_B = t f \pi \left(\frac{r_o + r_i}{2} \right)^2 \rho_m \quad (12)$$

where ρ_m is the copper mass density and m_B is the coil mass.

m_B is an important quantity since the coil is embedded in the mass in this analysis and so contributes to the total inertial mass (M) given by:

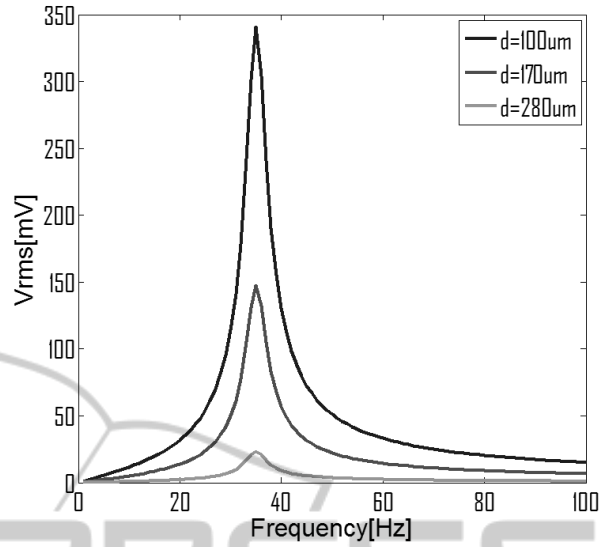
$$M = m + m_B \quad (13)$$

where m is the mass of the coil housing.

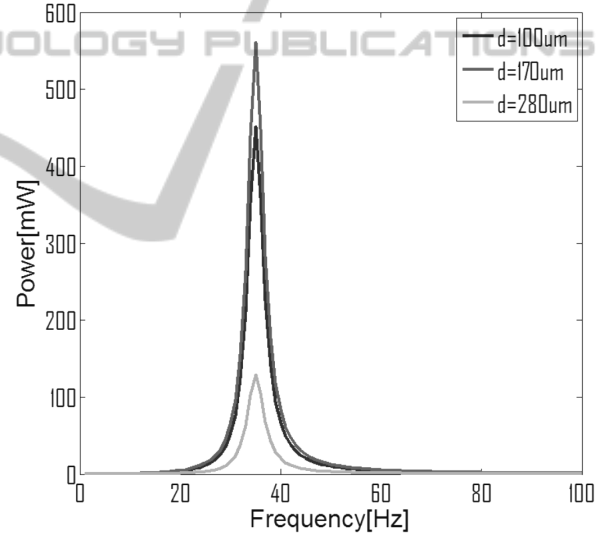
The system of equations has been solved with the Heun method, to avoid numerical divergence (Grasselli and Pelinovsky, 2008). The device is assumed to be in configuration (1) from Fig.1, with the smaller mass always attached to the springs.

The Power output has been calculated using $R_L = R_C$ and an effective spring constant has been calculated in order to match the experimental resonance frequency using the experimental value of the little mass (around 0.02 kg, slightly vaying with the mass of each coil).

Fig.5 shows simulation results for three different wire diameters for the 1DOF system with an input acceleration of $a=0.4g$. The results show that although



(a) Simulated voltage output with $RL=RC$ for the three coils



(b) Simulated power output with $RL=RC$ for the three coils
Figure 5: Simulation results in linear approximation for the transducer only.

the smallest wire diameter gives the highest voltage, the power is optimized using the intermediate wire diameter of $170 \mu\text{m}$. The ability to represent this type of effect is useful in order to ensure optimum coil parameters are found. The approach can also be extended to the analysis of multi-mass systems.

In the following section experimental results are used to verify that the optimum coil wire diameter found through simulation is correct for the actual systems of interest to this paper.

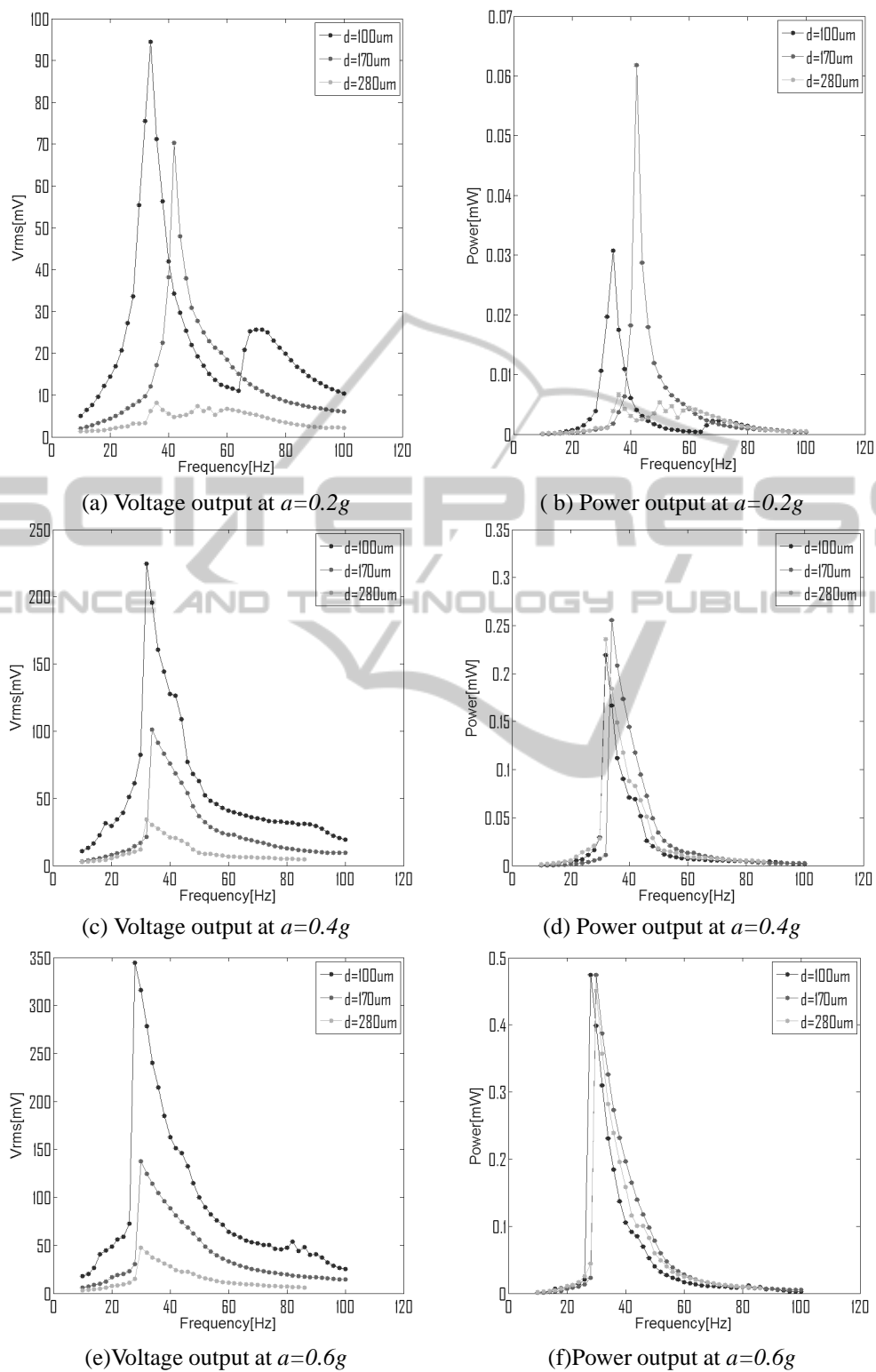


Figure 6: Voltage and power output comparison at different acceleration levels in configuration (1).

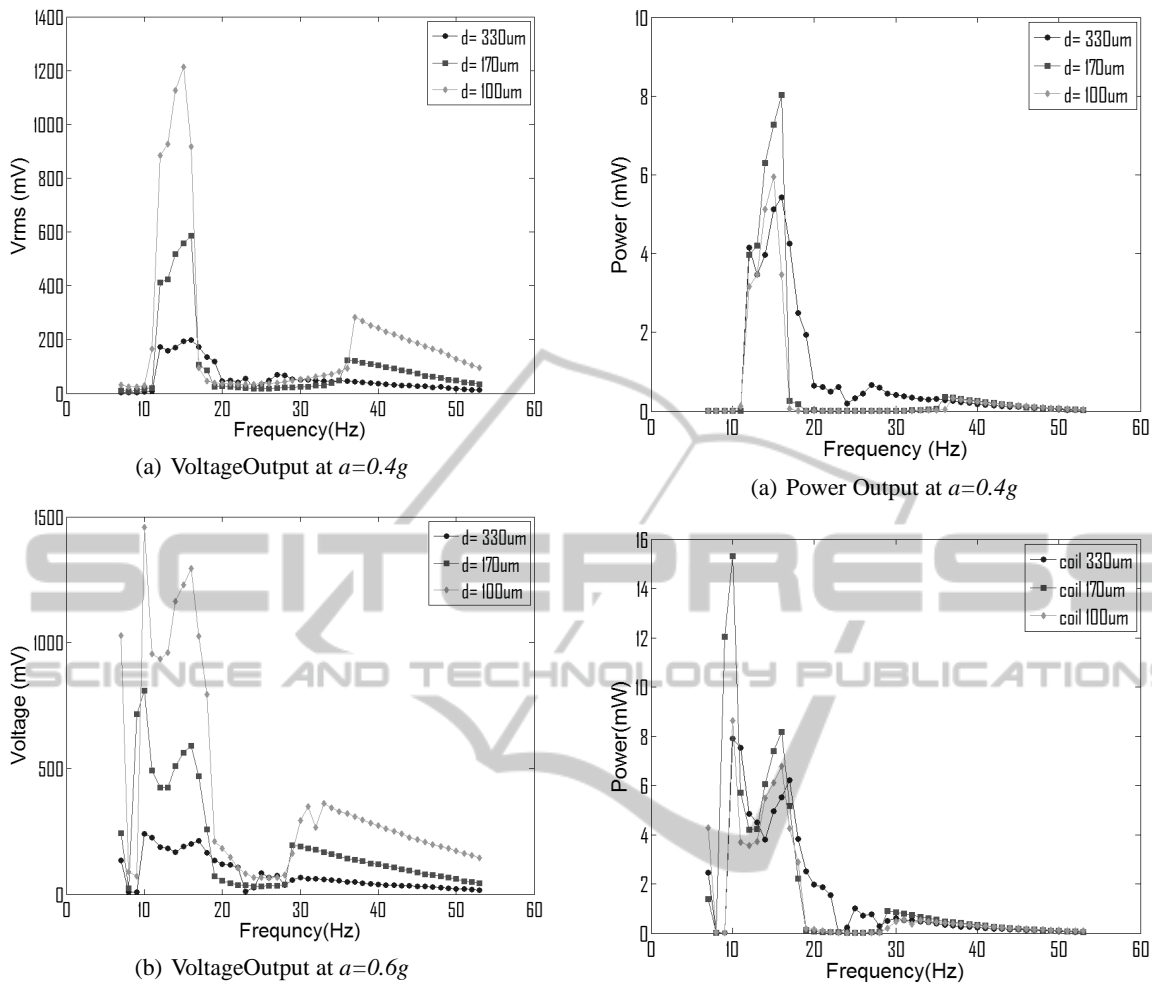


Figure 7: Voltage output for the three coils at different level of accelerations for configuration (3).

Figure 8: Power output for the three coils at different level of accelerations for configuration (3).

3.2 Experimental Validation of Optimum Coil Wire Diameter

The same experimental setup shown in Fig.2 was used to generate the results in this section. Configurations (1) and (3) from Fig.1 were tested. Three different wire diameters were analyzed in order to determine the most reasonable wire to use for winding the coil in terms of voltage and power output. The wire diameters selected were based on the modelling of the previous section and the experimental results serve to verify the model. Different levels of acceleration ($a=0.2g$, $a=0.4g$, $a=0.6g$) were provided as input to the two configurations of interest in order to verify that the optimal configuration did not change due to the frequency shifting observed in Section 2.3. In addition, three levels were imposed to show that the frequency shifting due to the system nonlinearity did not influence the optimal value of wire diameter.

The three coils used had the same volume, but they used different wire diameters of $100\mu m$, $170\mu m$ and $280\mu m$.

Each test was conducted by finding the optimal load resistance for the different coils and then measuring the voltage and power output. As a first stage, the system was optimized for configuration (1): the results are shown in Fig.6. Although the voltage output increases with decreasing wire diameter, the power output shows a maximum for the $170\mu m$ diameter, before decreasing again for the lowest wire diameter. This is due to the increasing resistance of the coil itself. The same effect is shown for increasing acceleration amplitude, as evident by comparing Fig.6 (d) and (f).

At $a=0.6g$ acceleration for configuration (1), the difference between the power output produced by the different coils reduces. This could be due to the fact

that the optimization theory is linear, which means that the system is required to maintain a fixed resonance frequency. This is clearly not true for a nonlinear system: the shifting in the frequency behaviour affects parameters such as the impedance of the coil, which is taken into account in the optimization. The same process was repeated for configuration (3) in Fig.1, in order to verify the same trends are observed in a multi-mass system which experiences the velocity amplification effect. In this case a wire diameter of $d=330\mu\text{m}$ was used instead of the $280\mu\text{m}$ diameter wire. Fig.7 and Fig.8 show that the optimal wire diameter is again $170\mu\text{m}$. The results also show that at $a=0.4g$, it is possible to see the two resonant peaks due to the two masses in motion. At $a=0.6g$, however, the nonlinearity of the whole system dominates, leading to just one large peak and the spectrum becomes wider.

The broadening of the resonance peak demonstrates an enhanced energy harvesting capability such that the system responds to a wider band of input frequencies. It is clear from the results that the model is capable of predicting the optimum wire diameter, indicating it is a useful design tool. Further improvements to the model would involve accounting for the insulation thickness in the coil and using a set of nonlinear equations to model the performance. These points will be addressed in future work.

4 CONCLUSIONS

In this paper, a 2DOF velocity amplified electromagnetic energy harvester has been presented. The nonlinearity occurring in the system for different configurations has been analyzed, which highlighted a softening nonlinearity. This feature has the effect of shifting the resonance frequencies of the harvester to lower values and to enlarge the bandwidth of the response. Thus it is possible to harvest energy from a wider band of frequencies, making it unnecessary to tune the harvester each time the driving frequency changes. The transfer function characterization also clearly demonstrates the gain in the output signal due to velocity amplification.

In the second part of the paper, an optimization model has been proposed, that is capable of predicting the most appropriate coil wire diameter for maximum voltage and/or power. The model employs a linear approximation, and it has been verified through comparison with three sets of data from different coils. The experimental tests were carried out using three levels of acceleration, and it was verified that the optimal coil configuration did not change substantially with the

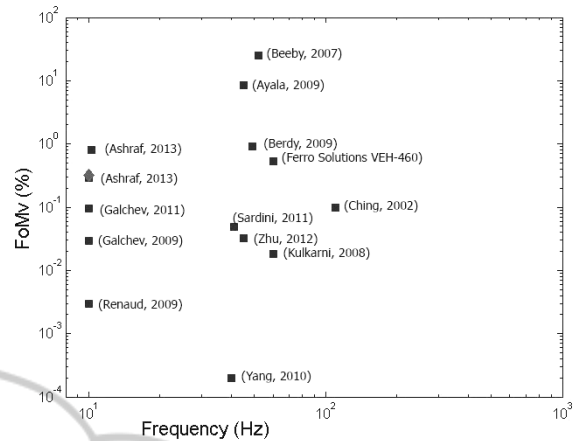


Figure 9: Comparison between recently published FoM (Ashraf et al., 2013a; Ashraf et al., 2013b; Galchev et al., 2011; Galchev et al., 2009; Renaud et al., 2009; Beeby et al., 2007; Ayala et al., 2009; Berdy et al., 2009; Ching et al., 2002; Sardini and Serpelloni, 2011; Zhu et al., 2012; Kulkarni et al., 2008; Yang and Lee, 2010). The diamond is our first prototype.

frequency shifting that occurs due to the nonlinearity of the system.

In Fig.9 the comparison with some recently reported energy harvesters in the literature is shown. A high Figure of Merit (FoM) (Mitcheson et al., 2008; Ashraf et al., 2013a) demonstrates the effectiveness of velocity amplification in electromagnetic energy harvesting. Until now, there has been no evidence of a finite lifetime of the analysed harvester due to mechanical failure, even with high accelerations. Future work will focus on improving the model accuracy through the introduction of a method to capture the effects of the nonlinearity of the multi-mass system. Moreover, the scaling down of the system will be addressed, in order to enable future integration on vibrating systems such as bridges or rotating machines.

ACKNOWLEDGEMENTS

The authors acknowledge the financial support of Science Foundation Ireland under Grant No. 10/CE/I1853 and the Irish Research Council (IRC) for funding under their Enterprise Partnership Scheme (EPS). This work was financially supported by the Industrial Development Agency (IDA) Ireland.

REFERENCES

Ashraf, Khir, Dennis, and Baharudin (2013a). Improved energy harvesting from low frequency vibrations by

- resonance amplification at multiple frequencies. In *Sensors and Actuators A: Physical*. ELSEVIER.
- Ashraf, Khir, Dennis, and Baharudin (2013b). A wide-band, frequency up-converting bounded vibration energy harvester for a low frequency environment. In *Smart Materials and Structures*. IOP Publishing.
- Ayala, Zhu, Tudor, and Beeby (2009). Autonomous tunable energy harvester. In *PowerMEMS, 2009*.
- Beeby, Torah, Tudor, Glynn-Jones, O'Donnell, Saha, and Roy (2007). A micro electromagnetic generator for vibration energy harvesting. In *Journal of Micromechanics and Microengineering*. IOP Publishing.
- Berdy, Srisungsthitthi, Xu, Rhoads, Jung, and Peroulis (2009). Compact low frequency meandered piezoelectric energy harvester. In *PowerMEMS, 2009*.
- Bouendeu, Greiner, Smith, and Korvink. (2011). Design synthesis of electromagnetic vibration-driven energy generators using a variational formulation. In *Journal of Microelectromechanical Systems*. IEEE.
- Ching, Wong, Li, Leong, and Wen (2002). A laser-micromachined multi-modal resonating power transducer for wireless sensing systems. In *Sensors and actuators A: Physical*. ELSEVIER.
- Cottone, Frizzell, Goyal, Kelly, and Punch (2014). Enhanced vibrational energy harvester based on velocity amplification. In *Journal of Intelligent Material Systems and Structures*. SAGE.
- Cottone, Vocca, and Gammaitoni (2009). Nonlinear energy harvesting. In *PhysRevLett, vol.102*. American Physical Society.
- Galchev, Cullagh, Peterson, and Najafi (2011). Harvesting traffic-induced vibrations for structural health monitoring of bridges. In *Journal of Micromechanics and Microengineering*. IOP Publishing.
- Galchev, Kim, and Najafi (2009). A parametric frequency increased power generator for scavenging low frequency ambient vibrations. In *Procedia Chemistry, Volume 1, Issue 1, September 2009, Pages 14391442*. ELSEVIER.
- Grasselli and Pelinovsky (2008). *Numerical Mathematics*. Jones & Bartlett Learning.
- Jang, Rustighi, Brennan, Lee, and Jung (2011). Design of a 2dof vibrational energy harvesting device. In *Journal of Intelligent Material Systems and Structures*. SAGE.
- Jang, Rustighi, Brennan, Lee, and Jung (2012). Vibration energy harvesting from random force and motion excitations. In *Journal of Intelligent Material Systems and Structures*. SAGE.
- Kulkarni, Koukharenko, Torah, Tudor, Beeby, O'Donnell, and Roy (2008). Design, fabrication and test of integrated micro-scale vibration-based electromagnetic generator. In *Sensors and Actuators A: Physical*. ELSEVIER.
- Leadenham and Erturk (2014). M-shaped asymmetric nonlinear oscillator for broadband vibration energy harvesting: Harmonic balance analysis and experimental validation. In *Journal of Sound and Vibration, vol.333, n.23, pag.6029-6223*. Elsevier.
- Mitcheson, Yeatmann, Rao, Holmes, and Green (2008). Energy harvesting from human and machine motion for wireless electronic devices. In *Proceedings of the IEEE*. IEEE.
- Mizuno and Chetwynd (2003). Investigation of a resonance microgenerator. In *Journal of Micromechanics and Microengineering 13, 209-216*. Institute of Physics Publishing.
- Muller and Massarani (2001). Transfer-function measurement with sweeps. In *J. Audio Eng. Soc.* AES.
- Nico, O'Donoghue, Frizzel, Kelly, and Punch (September 2014). A multiple degree-of-freedom velocity-amplified vibrational energy harvester part b: Modelling. In *ASME 2014 International Conference on Smart Materials*. SMASIS.
- O'Donoghue, Nico, Frizzel, Kelly, and Punch (September 2014). A novel velocity amplified vibrational energy harvester: Experimental analysis. In *ASME 2014 International Conference on Smart Materials*. SMASIS.
- Poulin, Sarraute, and Costa (2004). Generation of electrical energy for portable devices: Comparative study of an electromagnetic and a piezoelectric system. In *Sensors and Actuators A Physical*. ELSEVIER.
- Rebeiz, Regehr, Rutledge, Savage, and Jr, L. (1987). Submillimeter-wave antennas on thin membranes. In *International Journal of Infrared and Millimeter Waves*. Springer.
- Renaud, Fiorini, Schaijk, V., and Hoof, V. (2009). Harvesting energy from the motion of human limbs: the design and analysis of an impact-based piezoelectric generator. In *Smart Materials and Structures*. IOP Publishing.
- Sardini and Serpelloni (2011). An efficient electromagnetic power harvesting device for low-frequency applications. In *Sensors and actuators A: Physical*. ELSEVIER.
- Waters, Chisum, Jazo, and xFralick (2008). Development of an electro-magnetic transducer for energy harvesting of kinetic energy and its applicability to a mems-scale device. In *Nanopower Forum 2008*.
- Wheeler (1928). Simple inductance formulas for radio coils. In *Proceedings of the I.R.E.*
- Wheeler (1942). Formulas for the skin effect. In *Proceedings of the I.R.E.*
- Wu, Tang, Yang, and Soh (August 21, 2012b). A novel two-degree-of-freedom piezoelectric energy harvester. In *Journal of Intelligent Material Systems and Structures*. SAGE.
- Wu, Tang, Yang, and Soh (July 22, 2012a). Development of a broadband nonlinear two-degree-of-freedom piezoelectric energy harvester. In *Journal of Intelligent Material Systems and Structures*. SAGE.
- Yang and Lee (2010). Non-resonant electromagnetic wide-band energy harvesting mechanism for low frequency vibrations. In *Microsyst Technol (2010) 16:961966*. Springer-Verlag 2010.
- Zhu, Beeby, Tudor, and Harris (2012). Vibration energy harvesting using the halbach array. In *Smart Materials and Structures*. IOP Publishing.